Journal of Microscopy, Vol. 212, Pt 3 December 2003, pp. 273–279
Received 11 June 2003; accepted 20 June 2003

TectoRNA and 'kissing-loop' RNA: atomic force microscopy of self-assembling RNA structures

H. G. HANSMA, E. OROUDJEV, S. BAUDREY* & L. JAEGER*
*Department of Physics and *Department of Chemistry & Biochemistry, University of California, Santa Barbara, CA 93106, U.S.A.*

Key words. AFM, atomic force microscope, biomaterials, kissing-loop RNA, nanobiotechnology, scanning force microscopy, self-assembly, SFM, SPM, supramolecular assembly, tectoRNA.

Summary

RNA molecules have been much less studied by atomic force microscopy (AFM) than have DNA molecules. In this paper, AFM imaging is presented for two different RNA molecules able to self-assemble into complex supramolecular architectures. The first one is a molecular dimer of a 230-nt RNA fragment coming from the RNA genome of a murine leukaemia virus. The monomeric RNA fragment, which appears by AFM as an elongated structure with a mean aspect ratio of 1.4, assembles into a dimer of elongated structures through the formation of a 'kissing-loop' RNA interaction. The second one is a large supramolecular fibre formed of artificial self-assembling RNA molecular units called tectoRNA. The fibre lengths by AFM suggest that there are 50–70 tectoRNA units per fibre. Some methods and limitations are presented for measuring molecular volumes from AFM images.

Introduction

Atomic force microscopy (AFM) is a valuable tool for visualizing double- and single-stranded DNA and higher-order DNA structures. The first scanning-probe microscopic images of DNA were obtained in 1984 by looking at DNA strands on a silver-coated silicon chip with a scanning tunnelling microscope (Binnig & Rohrer, 1984; Binnig, 1992). Since 1992, DNA has been imaged extensively in many AFM studies in air, propanol and aqueous fluids (e.g. Bustamante *et al.*, 1992; Hansma *et al.*, 1992, 1993); in motion and in molecular and enzymatic processes, including DNase degradations (e.g. Bezanilla *et al.*, 1994; Ono & Spain, 1999); and transcription by RNA polymerase (Kasas *et al.*, 1997; Bustamante *et al.*, 1999). AFM of DNA has been a fruitful way to investigate DNA condensation, DNA–protein complexes and novel DNA structures (e.g. Golan *et al.*, 1999; Shlyakhtenko *et al.*, 2000; Yan *et al.*, 2002). For a recent review of AFM of DNA, see Hansma (2001).

More recently, AFM has been used as an invaluable tool for characterizing a variety of artificial three-dimensional (3D) nanoscale objects of defined topology (Winfree *et al.*, 1998; Sha *et al.*, 2002; Seeman, 2003). Some of the most striking AFM images are perhaps the images of self-organized DNA arrays from the Seeman and Winfree laboratories.

Despite an early start – RNA was also first imaged by AFM in 1992 (Henderson, 1992; Lyubchenko *et al.*, 1992) – RNA has been imaged by AFM much less extensively than DNA. In contrast to DNA, which is often regarded as a rather simple and monotonous helical structure, natural RNA molecules exhibit a breathtaking range of complex 3D structures that give rise to diverse functions (see, for example, Batey *et al.*, 1999; Ban *et al.*, 2000; Doudna, 2000; Yusupov *et al.*, 2001). Three of the more recent AFM studies of RNA are of catalytic RNA (ribozymes) transcribed from a rolling-circle template (Hansma *et al.*, 1999), and of a structural RNA component from bacteriophage phi29 (Trottier *et al.*, 2000; Mat-Arip *et al.*, 2001) and of RNA polymerase transcription complexes in which the nascent RNA can be seen (Rivetti *et al.*, 2003). One of the most exciting types of RNA imaging by AFM involves the observation of macromolecular complexes – apparently ribonucleoproteins containing messenger RNA – exiting from pores in the nuclear membrane (Oberleithner *et al.*, 2003).

Whereas DNA structures typically involve Watson–Crick base pairing, RNA has a greater diversity of tertiary interactions, often involving non-Watson–Crick base pairing. The two types of RNA molecules studied here are both capable of self-assembly, which provides exciting opportunities for the design of nanobiomaterials. These two RNAs self-assemble by either a 'kissing-loop' interaction or a loop-receptor interaction (for example, see Jaeger *et al.*, 1994; Costa & Michel, 1997; Wagner *et al.*, 2001; Brunel *et al.*, 2002). 'Kissing-loop' interactions involve Watson–Crick base pairing between

Correspondence: Dr H. Hansma. Tel.: +1 805 8933881; fax: +1 805 8938315; e-mail: hhansma@physics.ucsb.edu

complementary RNA loops. In contrast, loop–receptor interactions involve non-Watson–Crick base pairing.

The 'kissing-loop' RNA studied here is a 230-nt fragment from the Moloney murine leukaemia virus (MoMLV) genome that dimerizes through a palindromic loop sequence. This dimer is expected to hold together the two copies of the RNA genome during the replication process of this virus (Oroudjev *et al.*, 1999).

TectoRNAs have been defined as RNA Lego blocks that can assemble into supramolecular architectures (Westhof *et al.*, 1996; Jaeger & Leontis, 2000; Jaeger *et al.*, 2001). A fibre-forming tectoRNA has been studied here. In addition, we discuss the challenges of obtaining and analysing AFM images for these types of molecules.

Materials and methods

'Kissing-loop' RNAs

RNA samples were prepared, using the 230-nt MoMLV gRNA sequence pT(28–258) from the viral genome (Oroudjev *et al.*, 1999). PCR-generated template-DNA was transcribed using T7 RNA Polymerase. To purify newly produced RNA, the DNA template and T7 RNA Polymerase were removed from the reaction mix by RNAse-free DNAse treatment and phenol extraction. RNA was purified by electrophoresis on 2.5% low-melting-point agarose gel and stored at −80 °C. Before each use, purity and integrity of RNA samples were confirmed by electrophoresis on 6% and/or 12% PAGE.

To dimerize RNA samples, RNA at a concentration of 8 μM (600 μg mL^{-1}) was incubated in dimerization buffer (30 mM bistrispropane pH 7.6, 100 mM KCl, 10 mM $MgCl_2$) for 1 h at 37 °C. Dimerization was then stopped by placing the reaction tube on ice.

For AFM imaging, purified dimerized RNA was diluted 1 : 100 and 1 : 1000 in adsorption buffer (40 mM HEPES, pH 7.5, 10 mM $MgCl_2$). To image crude/unpurified RNA samples, total T7 RNA Polymerase reaction was diluted 1 : 100 in adsorption buffer. RNA samples prepared for imaging were then deposited on freshly cleaved mica, and RNA was allowed to adsorb to the mica surface for 3 min. The non-adsorbed RNA was removed from the mica surface by washing with DEPC-treated MilliQ-grade water (1–5 mL) and mica was dried in a stream of air. All images were collected in air with a MultiMode AFM and extended Nanoscope IIIa controller (Digital Instruments/Veeco, Santa Barbara, CA, U.S.A.).

TectoRNA

TectoRNA self-assembly was performed as described in Jaeger & Leontis (2000). Ten microlitres of 0.1 or 1 μM of RNA sample in 25 mM HEPES, pH 7.5, 15 mM $MgCl_2$, 100 mM KCl was then deposited on freshly cleaved mica for 3 min and washed with minimal volume of ultrapure water (~200 μL). RNA samples were then air dried (in a stream of dry helium) and imaged in 'tapping in air' mode on a Multimode AFM microscope equipped with a Nanoscope IIIa controller (Digital Instruments). All images were taken with MPP-11100 non-coated tapping/non-contact probe (resonance ~280 kHz, spring constant ~40 N m^{-1}) (Nanodevices, Santa Barbara, CA, U.S.A.).

Image analyses

Images were processed by flattening with the Nanoscope software (Digital Instruments/Veeco). Lengths, widths at half-height and heights were measured using the Section function in the Nanoscope off-line commands, with the Average Cursor. Molecular volumes were estimated using the Bearing function, by measuring the volume of the top half of the structure and multiplying by 2. The volume of the top half of the structure is the default presentation of data within a Bearing box. The Threshold feature of the software was set to 'On', for visualizing the x–y area covered by the top half of the structure.

Bend angles (α) in linear molecules were measured using the Height function in the NanoScope off-line commands. Molecular bends (β) – deviations from linearity – were calculated with the equation $\beta = 180° - \alpha$ (Rees *et al.*, 1993; Hansma, 2001). Bend angles can be measured more reliably by making measurements on molecules displayed with a colour table that defines a thin line running along the top edge of the fibre. The banded colour table 3 was used here, because it is better than the gradual brown/yellow colour table 2 in the NanoScope software.

Data are presented as means ± SD; n = number of molecules analysed. Widths are the widths at half-height.

Results

Results are presented for small data sets gathered from two RNA structures of interest to our group. We are extending this work primarily in the direction of continued imaging of tectoRNAs different from the tectoRNA presented here.

'Kissing-loop' RNAs

The 'kissing-loop' palindromic sequence involved in the dimerization of the 'kissing-loop' 230-nt RNA fragment is highlighted in Fig. 1. At low RNA concentration (Fig. 2A,C) clear isolated RNA structures are seen, whereas at a 10-fold higher concentration (Fig. 2B), the RNA structures are less well defined, and loose aggregates appear to be present. Figure 2(D,E) display structures of a 'kissing-loop' RNA mutant in which sequence GGU at nt's 205–207 was replaced with AAA (red bar, Fig. 1).

The individual elongated 'kissing-loop' structures observed by AFM had lengths of 23 ± 3 nm and aspect ratios (length/width) of 1.4 ± 0.2. Heights were 1.2 ± 0.2 nm.

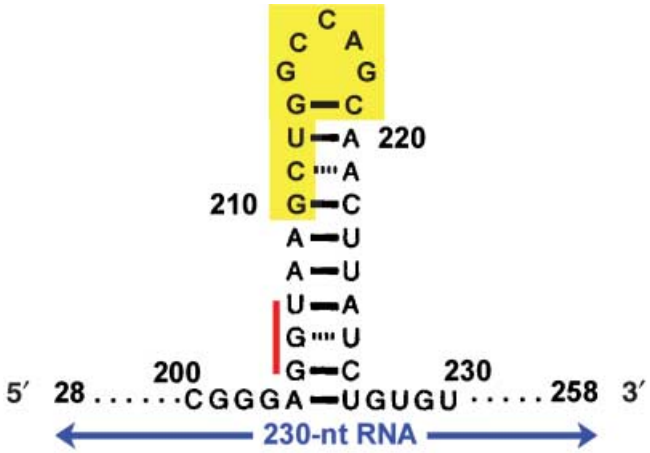

Fig. 1. Sequence of 'kissing-loop' hairpin within 230-nt RNA. Palindromic 'kissing-loop' sequence (blue) is located at nt's 210–220 of the 230-nt RNA shown by AFM in Fig. 2(A–C) (Oroudjev *et al.*, 1999). GGU sequence (red bar) at nt's 205–207 is mutated to AAA in the mutant RNA shown by AFM in Fig. 2(D–E). Numbering of nt's corresponds to the position of this RNA molecule in the MoMLV genome.

Some 'kissing-loop' structures appeared as double or triple blobs (arrows in Fig. 2A,D). The molecular volumes for single-blob structures were 139 ± 52 nm^3 ($n = 14$); the molecular volumes for double and triple-blob structures were 252 ± 64 nm^3 ($n = 6$). If the density of the RNA structures is 1 g mL^{-1}, this corresponds to mean masses of 83 kDa and 152 kDa for single-blob and multi-blob RNAs, respectively. If the density of the RNA structures is 1.3 g mL^{-1}, the mean masses are calculated to be 108 kDa and 197 kDa for single-blob and multi-blob RNAs, respectively.

TectoRNAs

In the presence of Mg^{2+}, the tectoRNA molecule 6 unit (Fig. 3A,B) has been shown by gel electrophoresis to multimerize into supramolecular structures composed of at least 15–20 units (Jaeger & Leontis, 2000). Interestingly, molecule 6 forms supramolecular fibres that were clearly visible by AFM (Fig. 3C). These fibres had apparent widths at half-height of 21 ± 4 nm, heights of 0.9 ± 0.1 nm ($n = 5$) and lengths of 140–250 nm.

The fibres had some bends as large as 40–50° from linear. Large bends were observed for example at the top of the question-mark-shaped fibre in Fig. 4 (arrows). Along most of their length, the fibres were relatively straight, deviating only 15° or less from linearity (Figs 3C and 4).

Volumes of the supramolecular fibres were estimated at 3050 ± 1480 nm^3. Fibre volumes per nanometre of fibre length were calculated to be 15 ± 4 nm^3 nm^{-1} contour length. This translates to a mean mass of 9 kDa nm^{-1} if the fibre density is 1 g mL^{-1} or 12 kDa nm^{-1} if the fibre density is 1.3 g mL^{-1}.

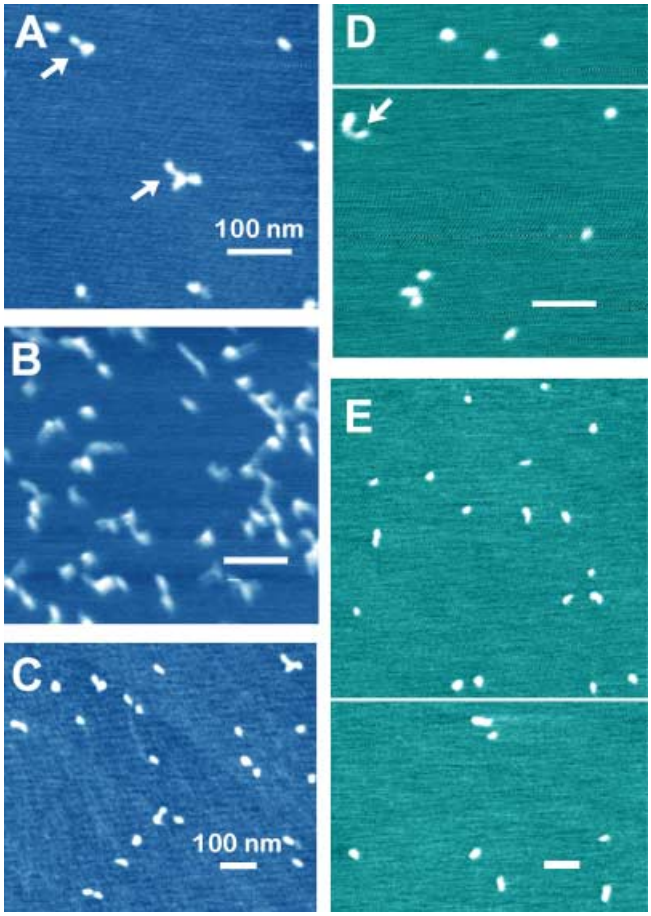

Fig. 2. 'Kissing-loop' RNAs. (A–C) Wild-type 'kissing-loop' RNAs (blue) at low (A,C) and high concentrations (B) (see Methods for details). (D,E) Mutant 'kissing-loop' RNAs (aquamarine) in which nt's 205–207 are changed from GGU to AAA. Regions from two AFM images are shown in (D) and in (E). Scale bars = 100 nm for all images.

Discussion

'Kissing-loop' RNAs

The objective of imaging the 'kissing-loop' RNAs was to observe the RNA monomer and the self-assembled dimer, seen previously only as bands on gels (Oroudjev *et al.*, 1999). RNA monomers and dimers from a bacteriophage have been observed previously with a cryo-AFM (Trottier *et al.*, 2000).

The most straightforward interpretation of the data in Fig. 2 is that single blobs are monomeric RNAs and double blobs are dimeric RNAs. The calculated molecular masses are reasonably consistent with this hypothesis, subject to the many uncertainties of obtaining reliable molecular masses from AFM volume measurements. The predicted molecular masses are ~75 kDa for monomeric RNAs and ~150 kDa for dimers, as calculated from the 230-nt RNA sequence. The mean molecular masses from AFM are 83 kDa for monomers and 152 kDa for dimers, assuming a blob density of 1 g mL^{-1}.

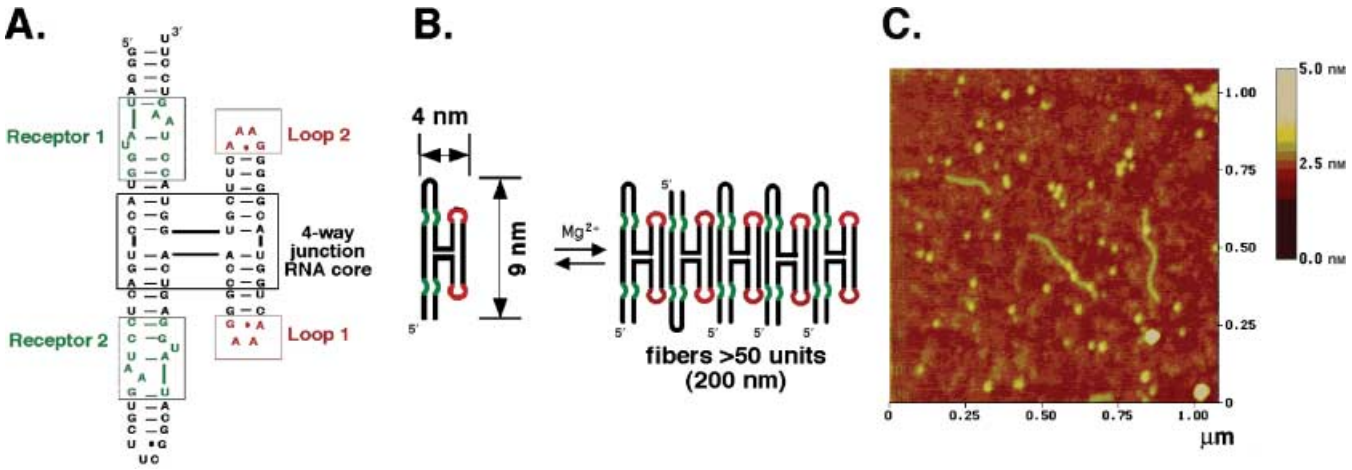

Fig. 3. TectoRNA design and image. (A) Sequence and secondary structure of tectoRNA molecule 6 (Jaeger & Leontis, 2000). (B) Diagram and dimensions of a single tectoRNA molecule and Mg^{2+}-dependent assembly into supramolecular fibres. Single RNA molecules can add to the fibre in either a head-to-tail or head-to-head orientation. (C) AFM image, in air, of three tecto-RNA supramolecular fibres. The sample for this image was prepared with 1 µM RNA. See Methods for further details.

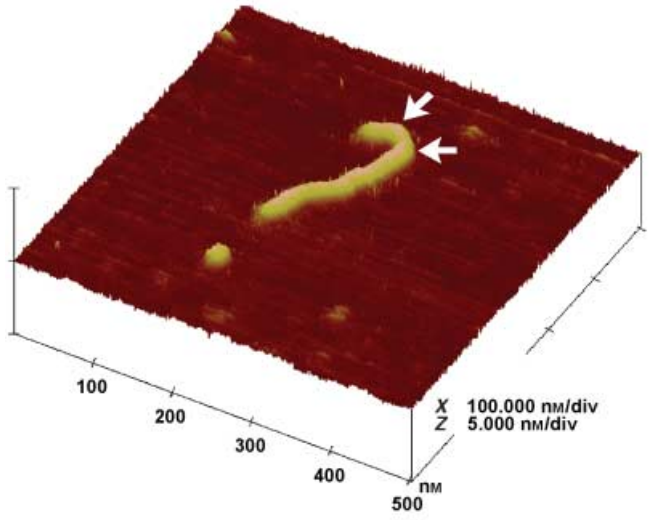

Fig. 4. Surface plot of a TectoRNA fibre. Arrows indicate positions of ~45° bends. Bends of this large size are thought to be due tectoRNAs that add to the fibre in a head-to-head direction. The sample for this image was prepared with 0.1 µM RNA. See Methods for further details.

Triple blobs and other large structures may be associations of three or more RNA molecules through a weaker association at sequences other than the 'kissing-loop' sequence. Larger structures were also seen sometimes by gel electrophoresis (E. Oroudjev, unpubl. data).

Under dimerization conditions, 50–60% of wild-type 'kissing-loop' RNAs dimerized, based on gel electrophoretic analysis (Oroudjev *et al.*, 1999). An RNA mutant outside the 'kissing loop' (red bar in Fig. 1) showed less dimerization that the wild-type RNA, by gel electrophoresis (E. Oroudjev, unpubl. data). AFM images of both wild-type and mutant seem to show somewhat less than 50% dimerization, suggesting that the RNA may denature somewhat when applied to the mica surface.

TectoRNAs

The modelled dimensions of the tectoRNA fibres are consistent with dimensions from AFM (Fig. 3B; Jaeger & Leontis, 2000), within the limitations of AFM dimension estimates. In the model, individual tectoRNA molecules are orientated with their long axes perpendicular to the fibre axis. Based on 3D modelling, tectoRNA molecule 6 has an overall size of 9 nm × 4 nm × 2 nm (L. Jaeger & N. B. Leontis, unpubl. data). The supramolecular fibre model has an overall diameter of ~10–12 nm, including the loops and stems of Fig. 3(B), or ~8–10 nm for only the thick core of the fibre. The tectoRNA fibres by AFM are wider and flatter than the modelled fibre. This is typical of AFM images, in which biomaterials appear to be compressed. The tectoRNA fibres had mean widths at half height of 21 nm and mean heights of 0.9 nm.

By comparison, both double- and triple-stranded DNA by AFM were only half as wide (10 ± 1 nm). Heights were 0.4 ± 0.1 nm for dsDNA and 0.7 ± 0.2 nm for tsDNA (Hansma *et al.*, 1996). X-ray diameters for dsDNA and tsDNA are 2–3 nm. As expected, AFM imaging is compatible with the model that tectoRNA fibres are wider and higher than either dsDNA or tsDNA.

The molecular mass of molecule 6 is 29 kDa, based on its sequence. The fibres by AFM had mean masses of 9–12 kDa nm^{-1}, based on fibre densities of 1–1.3 g mL^{-1}. These fibre masses of 9–12 kDa per nm length are 30–40% of the 29-kDa mass of individual tectoRNA molecules. As the individual molecules have short dimensions of 2 nm × 4 nm, 1 nm of fibre length might be expected to contain *c.* 25–50% of an individual

tectoRNA molecule. The fibre masses estimated from AFM volumes predict that 1 nm of fibre length contains ~31–41% of an individual tectoRNA molecule. Furthermore, a fibre 250 nm in length is predicted to have 75–100 tectoRNA units.

The tectoRNA molecules in Figs 3 and 4 assemble into fibres in two different orientations, such that individual molecules can add to the fibre in either a head-to-tail or a head-to-head fashion. The individual molecules can add to the fibre in two directions because the two loops and the two receptors on each molecule are identical (Fig. 3A,B).

Modelling of these fibres shows that head-to-tail addition of RNA molecules produces a linear fibre, whereas head-to-head additions of RNA molecules produces either a bend or a fibre termination (L. Jaeger & N. B. Leontis, unpubl. data). Therefore, these fibres are predicted to have bends. Bends of up to 45° were observed by AFM of these fibres (e.g. arrows in Fig. 4). Fibres of tectoRNA 6 have also been seen by TEM. Interestingly, these fibre images also display some bends (N. B. Leontis & L. Jaeger, unpubl. data). The bends are attributed to the head-to-head additions of tectoRNA molecules at the positions of the bends during fibre assembly.

Estimating macromolecular volumes by AFM

AFM images provide tantalizing information about the volumes of molecular structures. The volumes of known structures in AFM images correspond reasonably well to the molecular masses of the structures, assuming a density in the range 1–1.3 g mL^{-1} (Schneider *et al.*, 1998; Golan *et al.*, 1999; Hansma *et al.*, 2002). There are, however, many uncertainties in accurately extracting volume information from AFM images.

The tip convolution is an obvious and large uncertainty that has been extensively analysed to develop ways of deconvoluting the tip from the sample, based on imaging and analysis of known samples. Even a perfect tip deconvolution will not be able to calculate the volume of any 'empty space' under the sides of a structure. For example, an AFM image of a hard sphere on a surface has much 'empty space' beneath the lower half of the sphere. Conveniently, biomaterials are soft and will therefore conform to the surface better than a rigid object, thus reducing the volume of empty space. Another uncertainty in volume measurements is that the AFM tip can become sharper or blunter between one image and the next if it gains or loses material.

Therefore, it is often practical to use directly the AFM volume data for estimating volumes of molecules and other structures. The approach used in this paper (Fig. 5A) is one of three related approaches that we have used for various biomaterials. This approach is to assume that the volume of the top half of the structure within the box is half of the volume of the entire structure. (Fig. 5A; see also Methods.) This approach does not require subjective input, but it depends strongly on the height/depth of the highest/lowest pixel in the image, as seen from the histogram in Fig. 5(A).

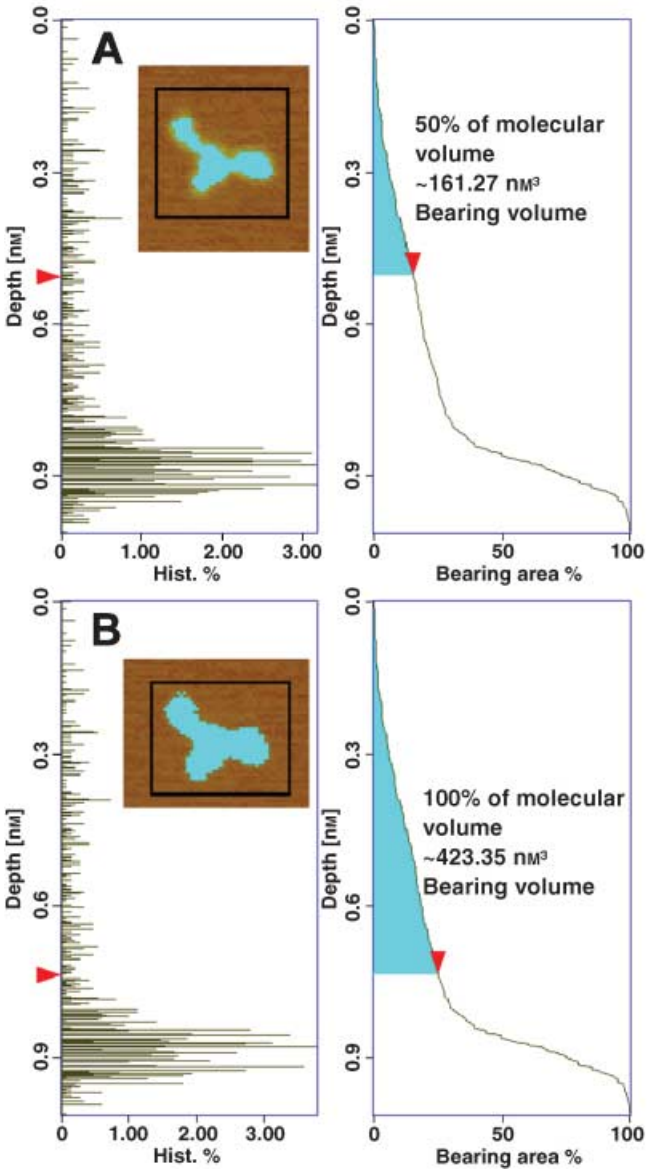

Fig. 5. Two methods of estimating volume from AFM software. The RNA structure can be seen also in the centre of Fig. 2(A). (A) This method assumes that half of the volume of the molecule or structure is present at sample depths of 0–50% of the deepest point of the sample. The cursor (red) appears here by default in the Nanoscope bearing software. This method is objective but is likely to be inaccurate if the structure has height asymmetries (see Fig. 6A) or if there are exceptionally low pixels in the background (i.e. pixels at a large depth in the left panel) or exceptionally high pixels in the structure (i.e. pixels at a small depth in the left panel). (B) This method assumes that the volume of the molecule or structure is present at all sample depths higher than the sample surface. A user-defined position of the cursor (red) makes this method subjective. This method is also likely to over-estimate the molecular volume owing to contributions from the tip volume, but this method is probably better for structures with asymetric heights, as in Fig. 6(A).

Previously, we have also used two other approaches for estimating molecular volumes directly from the volume data in AFM images. One of these approaches involves a background subtraction and has been described previously (Hansma *et al.*, 2002). The other approach is presented in Fig. 5(B). This approach is to assume that the total volume of the molecule is comparable to the volume above the bell-curve of the histogram, based on a user-defined position for the boundary between the bell-curve and the region above the bell curve (Fig. 5B). The large bell-curve in the histograms of Fig. 5(A,B) (left panels) corresponds to the background in the box, and the rest of the histogram, at smaller depths, corresponds roughly to the volume of the molecule.

By comparing the molecular volume estimates in Fig. 5(A,B), one can see that the estimate in Fig. 5(A) (323 nm^3) is 76% of the estimate in Fig. 5(B) (423 nm^3). The smaller volume estimate in Fig. 5(A) is probably due to the fact that a conical tip contributes to the apparent volume of the molecule in proportion to the length of the tip that is in contact with the sample. This is one reason for the interest in high-aspect-ratio carbon-nanotube AFM tips.

Any volume analysis also needs intelligent observation. For example, the threshold feature of AFM software is a useful assistant in assessing the reliability of volume measurements. As shown in Fig. 6(A,B), the threshold distinguishes between structures with symmetric heights (Fig. 6B) and structures with asymmetric heights (Fig. 6A).

The precision of volume measurements can be deceptive, because the AFM software presents all data at four or five significant figures, regardless of the number of pixels actually present in the object being measured. There are, for example, only 7–9 pixels in each 'kissing-loop' RNA structure in a 2-μm scan at 256 pixels per line, but a typical volume is given as 96.214 nm^3. The 'kissing-loop' RNA measurements analysed here were taken from 0.5-μm scans, giving a four-fold increase in precision.

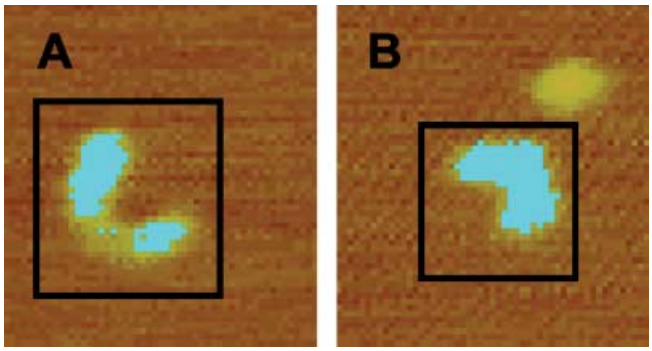

Fig. 6. Using a threshold to aid in volume estimates in order to distinguish between asymmetric (A) and asymmetric (B) heights. The threshold is placed at 50% of the sample depth as in Fig. 5(A). The RNA structures can be seen also in Fig. 2(D). (A) This structure has an asymmetric height. Therefore, the low region between the two blue areas is totally excluded from a volume estimate based on twice the volume of the top half. A better approach might be to use the method of Fig. 5(B). (B) The volume of this structure can probably be estimated reasonably well as twice the volume of the top half.

Volume estimates are most useful when accuracy at the level of ±~50% is sufficient. According to Pietrasanta *et al.* (1999), volume estimates were not useful for determining the stoichiometry of a centromeric DNA–protein complex, when the question was whether there were ~four, five or six protein molecules per complex. But volume estimates were useful in the same study for predicting whether four-armed DNA–protein complexes contained approximately as much protein as two two-armed DNA–protein complexes. Volume estimates were also useful for predicting the composition of DNA toroids (Golan *et al.*, 1999) and for predicting the substructure of nanofibres from a spider dragline-silk protein (Oroudjev *et al.*, 2002, 2003).

Conclusion

These results are the beginning of an extensive project aimed at visualizing and characterizing by AFM new tectoRNA molecules and new supramolecular tectoRNA structures. These tectoRNAs, like DNA, have potential as self-assembling programmable biomaterials with applications in nanobiotechnology (Jaeger *et al.*, 2001; Seeman, 2003). The prospects of generating 2D arrays of tectoRNAs also provide strong impetus to improve AFM sample preparation and imaging by developing new techniques for good RNA adsorption without denaturation and by working with the best possible AFMs, tips and cantilevers.

Acknowledgement

This work was funded by NSF MCB grants to H.H. and by a seed grant from the UCSB Materials Research Laboratory, funded by NSF MRSEC DMROO-80034 to L.J.

References

Ban, N., Nissen, P., Hansen, J., Moore, P.B. & Steitz, T.A. (2000) The complete atomic structure of the large ribosomal subunit at 2.4 A resolution [see comments]. *Science*, **289**, 905–920.

Batey, R.T., Rambo, R.P. & Doudna, J.A. (1999) Tertiary motifs in RNA structure and folding. *Angew Chem. Int. Ed. Engl.* **38**, 2326–2343.

Bezanilla, M., Drake, B., Nudler, E., Kashlev, M., Hansma, P.K. & Hansma, H.G. (1994) Motion and enzymatic degradation of DNA in the atomic force microscope. *Biophys. J.* **67**, 2454–2459.

Binnig, G. (1992) Force microscopy. *Ultramicroscopy*, **42–44**, 7–15.

Binnig, G. & Rohrer, H. (1984) Scanning tunneling microscopy. *Trends in Physics* (ed. by J. Janta and J. Pantoflicek), pp. 38–46. European Physical Society, The Hague.

Brunel, C., Marquet, R., Romby, P. & Ehresmann, C. (2002) RNA loop–loop interactions as dynamic functional motifs. *Biochimie*, **84**, 925–944.

Bustamante, C., Guthold, M., Zhu, X. & Yang, G. (1999) Facilitated target location on DNA by individual *Escherichia coli* RNA polymerase molecules observed with the scanning force microscope operating in liquid. *J. Biol. Chem*. **274**, 16665–16668.

Bustamante, C., Vesenka, J., Tang, C.L., Rees, W., Guthold, M. & Keller, R. (1992) Circular DNA molecules imaged in air by scanning force microscopy. *Biochemistry*, **31**, 22–26.

Costa, M. & Michel, F. (1997) Rules for RNA recognition of GNRA tetraloops deduced by in vitro selection: comparison with in vivo evolution. *EMBO J*. **16**, 3289–3302.

Doudna, J.A. (2000) Structural genomics of RNA. *Nat. Struct. Biol*. **7** (Suppl.), 954–956.

Golan, R., Pietrasanta, L.I., Hsieh, W. & Hansma, H.G. (1999) DNA toroids: stages in condensation. *Biochemistry*, **38**, 14069–14076.

Hansma, H.G. (2001) Surface biology of DNA by atomic force microscopy. *Annu. Rev. Phys. Chem*. **52**, 71–92.

Hansma, H.G., Bezanilla, M., Zenhausern, F., Adrian, M. & Sinsheimer, R.L. (1993) Atomic force microscopy of DNA in aqueous solutions. *Nucl. Acids Res*. **21**, 505–512.

Hansma, H.G., Clegg, D.O., Kokkoli, E., Oroudjev, E. & Tirrell, M. (2002) Analysis of matrix dynamics by atomic force microscopy. *Methods in Cell Biology* (ed. by J. Adams), pp. 163–193. Academic Press, San Diego.

Hansma, H.G., Golan, R., Hsieh, W., Daubendiek, S.L. & Kool, E.T. (1999) Polymerase activities and RNA structures in the atomic force microscope. *J. Struct. Biol*. **127**, 240–247.

Hansma, H.G., Revenko, I., Kim, K. & Laney, D.E. (1996) Atomic force microscopy of long and short double-stranded, single-stranded and triple-stranded nucleic acids. *Nucl. Acids Res*. **24**, 713–720.

Hansma, H.G., Vesenka, J., Siegerist, C., Kelderman, G., Morrett, H., Sinsheimer, R.L., Bustamante, C., Elings, V. & Hansma, P.K. (1992) Reproducible imaging and dissection of plasmid DNA under liquid with the atomic force microscope. *Science*, **256**, 1180–1184.

Henderson, E. (1992) Atomic force microscopy of conventional and unconventional nucleic acid structures. *J. Microsc.* **167**, 77–84.

Jaeger, L. & Leontis, N.B. (2000) Tecto-RNA: one-dimensional self–assembly through tertiary interactions. *Angew Chem. Int. Ed.* 2521–2524.

Jaeger, L., Michel, F. & Westhof, E. (1994) Involvement of a GNRA tetraloop in long–range RNA tertiary interactions. *J. Mol. Biol*. **236**, 1271–1276.

Jaeger, L., Westhof, E. & Leontis, N.B. (2001) TectoRNA: modular assembly units for the construction of RNA nano-objects. *Nucl. Acids Res*. **29**, 455–463.

Kasas, S., Thomson, N.H., Smith, B.L., Hansma, H.G., Zhu, X., Guthold, M., Bustamante, C., Kool, E.T., Kashlev, M. & Hansma, P.K. (1997) *E. coli* RNA polymerase activity observed using atomic force microscopy. *Biochemistry*, **36**, 461–468.

Lyubchenko, Y.L., Jacobs, B.L. & Lindsay, S.M. (1992) Atomic force microscopy of reovirus dsRNA: a routine technique for length measurements. *Nucl. Acids Res*. **20**, 3983–3986.

Mat-Arip, Y., Garver, K., Chen, C., Sheng, S., Shao, Z. & Guo, P. (2001) Three–dimensional interaction of Phi29 pRNA dimer probed by chemical modification interference, cryo-AFM, and cross-linking. *J. Biol. Chem*. **276**, 32575–32584.

Oberleithner, H., Schafer, C., Shahin, V. & Albermann, L. (2003) Route of steroid-activated macromolecules through nuclear pores imaged with atomic force microscopy. *Biochem. Soc. Trans*. **31**, 71–75.

Ono, M.Y. & Spain, E.M. (1999) Dynamics of DNA condensates at the solid–liquid interface by atomic force microscopy. *J. Am. Chem. Soc*. **121**, 7330–7334.

Oroudjev, E., Hayashi, C.Y., Soares, J., Arcidiacono, S., Fossey, S.A. & Hansma, H.G. (2003) Nanofiber formation in spider dragline-silk as probed by atomic force microscopy and molecular pulling. *Mat. Res. Soc. Symp. Proc*. **738**, G.10.4.1–G.10.4.7.

Oroudjev, E.M., Kang, P.C.E. & Kohlstaedt, L.A. (1999) An additional dimer linkage structure in moloney murine leukemia virus RNA. *J. Mol Biol*. **291**, 603–613.

Oroudjev, E., Soares, J., Arcidiacono, S., Thompson, J.B., Fossey, S.A. & Hansma, H.G. (2002) Segmented nanofibers of spider dragline silk. Atomic force microscopy and single-molecule force spectroscopy. *Proc. Natl Acad. Sci. USA*, **99**, 6460–6465.

Pietrasanta, L.I., Thrower, D., Hsieh, W., Rao, S., Stemmann, O., Lechner, J., Carbon, J. & Hansma, H.G. (1999) Probing the *Sacchromyces cervisiae* CBF3-*CEN* DNA kinetochore complex using atomic force microscopy. *Proc. Natl Acad. Sci. USA*, **96**, 3757–3762.

Rees, W.A., Keller, R.W., Vesenka, J.P., Yang, C. & Bustamante, C. (1993) Evidence of DNA bending in transcription complexes imaged by scanning force microscopy. *Science*, **260**, 1646–1649.

Rivetti, C., Codeluppi, S., Dieci, G. & Bustamante, C. (2003) Visualizing RNA extrusion and DNA wrapping in transcription elongation complexes of bacterial and eukaryotic RNA polymerases. *J. Mol. Biol*. **326**, 1413–1426.

Schneider, S.W., Larmer, J., Henderson, R.M. & Oberleithner, H. (1998) Molecular weights of individual proteins correlate with molecular volumes measured by atomic force microscopy. *Pflugers Arch*. **435**, 362–367.

Seeman, N.C. (2003) DNA in a material world. *Nature*, **421**, 427–431.

Sha, R., Liu, F. & Seeman, N.C. (2002) Atomic force microscopic measurement of the interdomain angle in symmetric Holliday junctions. *Biochemistry*, **41**, 5950–5955.

Shlyakhtenko, L.S., Hsieh, P., Grigoriev, M., Potaman, V.N., Sinden, R.R. & Lyubchenko, Y.L. (2000) A cruciform structural transition provides a molecular switch for chromosome structure and dynamics. *J. Mol. Biol*. **296**, 1169–1173.

Trottier, M., Mat-Arip, Y., Zhang, C., Chen, C., Sheng, S., Shao, Z. & Guo, P. (2000) Probing the structure of monomers and dimers of the bacterial virus phi29 hexamer RNA complex by chemical modification. *RNA*, **6**, 1257–1266.

Wagner, C., Palacios, I., Jaeger, L., St Johnston, D., Ehresmann, B., Ehresmann, C. & Brunel, C. (2001) Dimerization of the 3′UTR of bicoid mRNA involves a two-step mechanism. *J. Mol. Biol*. **313**, 511–524.

Westhof, E., Masquida, B. & Jaeger, L. (1996) RNA tectonics: towards RNA design. *Structure, Folding Design*, **1**, 78–88.

Winfree, E., Liu, F., Wenzler, L.A. & Seeman, N.C. (1998) Design and self-assembly of two-dimensional DNA crystals. *Nature*, **394**, 539–544.

Yan, H., Zhang, X., Shen, Z. & Seeman, N.C. (2002) A robust DNA mechanical device controlled by hybridization topology. *Nature*, **415**, 62–65.

Yusupov, M.M., Yusupova, G.Z., Baucom, A., Lieberman, K., Earnest, T.N., Cate, J.H. & Noller, H.F. (2001) Crystal structure of the ribosome at 5.5 A resolution. *Science*, **292**, 883–896.